Modeling of short-pulse generation by Yb^{3+}:YAG crystal in an active continuous-wave-injected ring cavity using different end-pump methods

Zhiyun Huang,* Gaoming Li, and Yishen Qiu

Key Laboratory of Optoelectronic Science and Technology for Medicine, Ministry of Education, School of Physics and OptoElectronics Technology, Fujian Normal University, Fuzhou, Fujian 350007, China
**Corresponding author: zhiyunhuang@fjnu.edu.cn*

Received January 18, 2008; revised May 23, 2008; accepted July 1, 2008;
posted July 15, 2008 (Doc. ID 91745); published August 15, 2008

Using different end-pump methods, short-pulse generation in an active continuous-wave-injected ring cavity with homogeneously broadened Yb^{3+}:YAG crystal is studied numerically. In the derived model, the saturation of the pump absorption is taken into account. The effects of the seeding intensity, the seeding frequency, the amplifier length, and the efficiency of the acousto-optic modulator on the peak intensity using different end-pump methods are analyzed. The results show that, of the end-pump methods considered, the optimum method is the backreflection pump method. © 2008 Optical Society of America

OCIS codes: 140.3280, 140.3580, 140.5680.

1. INTRODUCTION

Yb^{3+}-doped laser materials are of great interest since high-power InGaAs laser diodes are used as pump sources. Compared with their Nd^{3+}-doped counterparts, Yb^{3+}-doped laser materials have many advantages and can be used as the gain medium of a diode-pumped high-power solid-state laser [1,2]. Among them, Yb^{3+}:YAG ($Yb^{3+}:Y_3Al_5O_{12}$) crystal has good thermomechanical properties and has worked as the amplifier medium in short-pulse lasers [1–3].

In many fields, such as coherent lidar for ranging and pollution detection, chemistry, and biology, a laser pulse with known frequency is needed. For this purpose, a method for obtaining a short laser pulse from an active continuous-wave-injected ring laser cavity was demonstrated [4,5]. In that method, the frequency of the pulse can be controlled by that of the seeding laser, and the pulse duration can be controlled by the intensity of the rf signal driving the acousto-optic modulator (AOM). Moreover, to increase the energy of the resulting laser pulse, an amplifier can be inserted into the ring cavity [5,6].

In a previous paper [6], the effects of the seeding intensity, the seeding frequency, and the amplifier length were studied. Furthermore, developed from the previous paper, the model taking into account the saturation of the pump absorption is derived in this paper. By using the formulas, the performance of the laser pulse under different end-pump methods is studied.

2. SHORT-PULSE GENERATION

Figure 1 shows the scheme of the ring cavity studied in this paper. The energy diagram of the Yb^{3+}:YAG crystal is shown in Fig. 2, where f_{li}, f_{uj}, f_{lm}, and f_{un} represent the Boltzmann factors of the corresponding Stark levels. Then the rate equation under steady state for the Yb^{3+}:YAG crystal in the cavity is [7]

$$\tau_f \frac{dX_u(z)}{dt} = \beta_p(z)[f_p - X_u(z)] - X_u(z) - [X_u(z) - f_l]\sum_n \beta(\nu_n, z) = 0, \quad (1)$$

where z is the longitudinal coordinate, and in the above equation, the transverse coordinate is not considered. ν_p and ν_n are the frequencies of the pump and laser beams with $\nu_n = \nu_0 + n\,\delta\nu$ $(n = 0, 1, 2, \ldots)$ and ν_0 is the frequency of the seeding laser, $\delta\nu$ is the frequency shift generated by the AOM, and the sum takes over all the frequencies existing in the amplifier. $\beta_p(z)$ and $\beta(\nu_n, z)$ are the intensities normalized to their saturation intensity with $\beta_p(z) = I_p(z)/I_{ps}$ and $\beta(\nu_n, z) = I(\nu_n, z)/I_s(\nu_n)$, respectively, where $I_p(z)$ and $I(\nu_n, z)$ are the pump and laser intensities and I_{ps} and $I_s(\nu_n)$ are the pump and laser saturation intensities with $I_{ps} = h\nu_p/(f_{li} + f_{uj})\tau_f\sigma_p$ and $I_s(\nu_n) = h\nu_n/(f_{lm} + f_{un})\tau_f\sigma_e(\nu_n)$, respectively, where τ_f is the fluorescence lifetime of the upper laser level, σ_p is the absorption cross section for the pump beam, $\sigma_e(\nu_n)$ is the emission cross section for the laser beam of frequency ν_n, and h is Planck's constant. $X_u(z) = N_u(z)/N_0$, where $N_u(z)$ is the population density of upper manifold, N_0 is the Yb^{3+} concentration. The parameters f_p and f_l are defined as $f_p = f_{li}/(f_{li} + f_{uj})$ and $f_l = f_{lm}/(f_{lm} + f_{un})$.

From Eq. (1), the value of $X_u(z)$ is

 © 2008 Optical Society of America

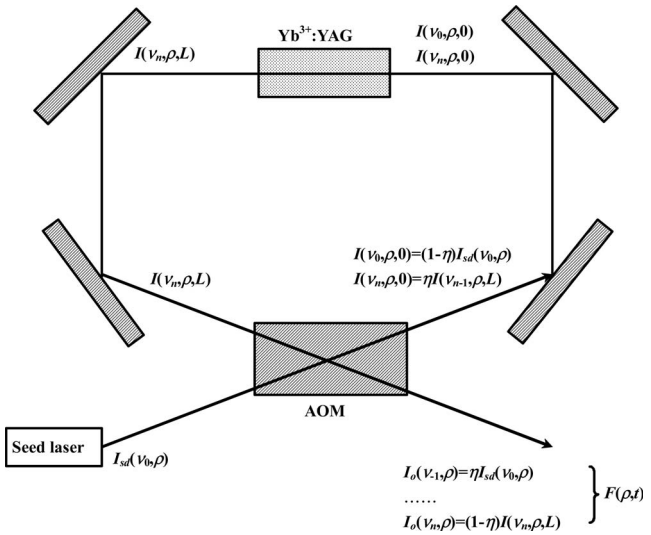

Fig. 1. Scheme of the ring cavity with Yb^{3+}:YAG crystal.

$$X_u(z) = \frac{f_p\beta_p(z) + f_l\Sigma_n\beta(\nu_n,z)}{1 + \beta_p(z) + \Sigma_n\beta(\nu_n,z)}. \quad (2)$$

The inversion population density $\Delta N(z)$ and the population participating in the pump process $\Delta N_p(z)$ are

$$\Delta N(z) = (f_{lm} + f_{un})[X_u(z) - f_l]N_0, \quad (3a)$$

$$\Delta N_p(z) = (f_{li} + f_{uj})[f_p - X_u(z)]N_0. \quad (3b)$$

For the homogeneously broadened amplifier, the intensity $I(\nu_n,z)$ and the pump intensity are

$$\frac{1}{I(\nu_n,z)}\frac{dI(\nu_n,z)}{dz} = \frac{1}{\beta(\nu_n,z)}\frac{d\beta(\nu_n,z)}{dz} = g(\nu_n)[X_u(z) - f_l], \quad (4a)$$

$$\frac{1}{I_p^{\pm}(z)}\frac{dI_p^{\pm}(z)}{dz} = \frac{1}{\beta_p^{\pm}(z)}\frac{d\beta_p^{\pm}(z)}{dz} = \mp\alpha_p[f_p - X_u(z)], \quad (4b)$$

where $g(\nu_n)=\sigma_e(\nu_n)(f_{lm}+f_{un})N_0$, $\alpha_p=\sigma_p(f_{li}+f_{uj})N_0$, $I_p^+(z)$ and $I_p^-(z)$ are the pump intensity propagating along $\pm z$ direction, and the pump intensity is $I_p(z)=I_p^+(z)+I_p^-(z)$. In Eq. (4a), the internal loss in the amplifier is neglected. From Eqs. (4a) and (4b), it is obvious that

$$\frac{1}{I(\nu_n,z)}\frac{dI(\nu_n,z)}{dz} = g(\nu_n)\left[(f_p - f_l) \pm \frac{1}{\alpha_p I_p^{\pm}(z)}\frac{dI_p^{\pm}(z)}{dz}\right]. \quad (5)$$

In Eq. (5), let $\nu_n = \nu_0$. Then integrating Eq. (5) from 0 to z gives

$$G(\nu_0,z) = g(\nu_0)\left[(f_p - f_l)z \pm \frac{G_p^{\pm}(z)}{\alpha_p}\right],$$

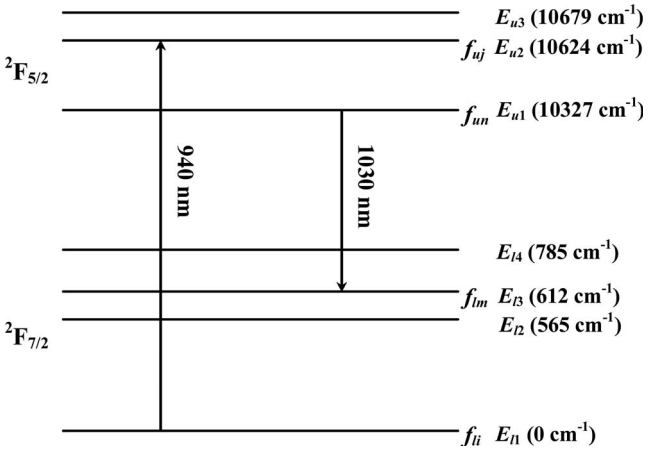

Fig. 2. Energy diagram of the Yb^{3+}:YAG crystal.

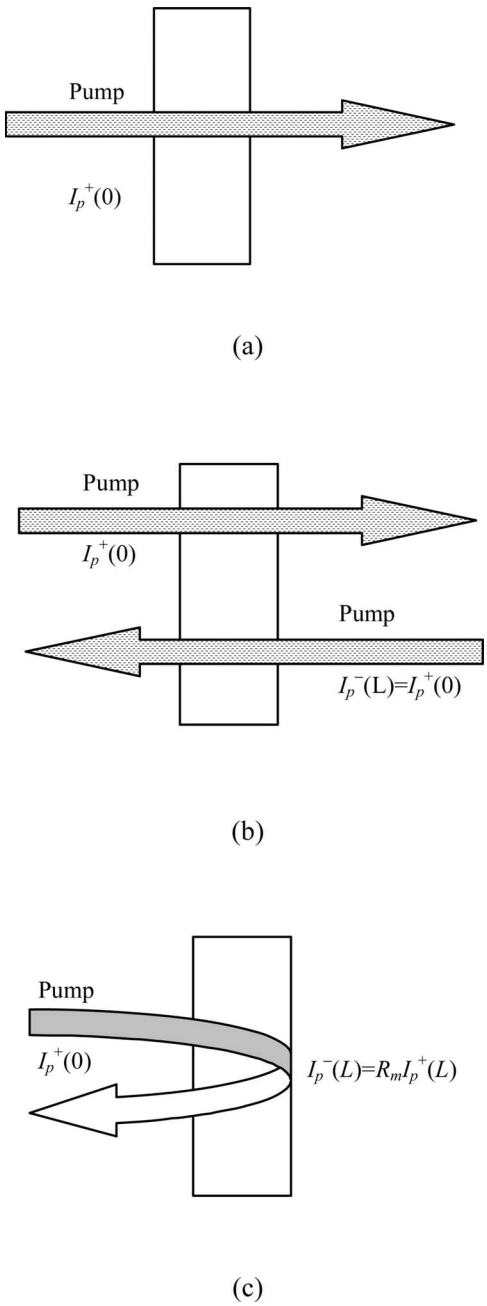

Fig. 3. Three different pump methods: (a) single-pass pump, (b) contrapropagating pump, (c) backreflection pump.

$$G(\nu_0,z)=\ln\frac{I(\nu_0,z)}{I(\nu_0,0)}=\ln\frac{\beta(\nu_0,z)}{\beta(\nu_0,0)},$$

$$\Gamma_p^{\pm}(z)=\ln\frac{I_p^{\pm}(z)}{I_p^{\pm}(0)}=\ln\frac{\beta_p^{\pm}(z)}{\beta_p^{\pm}(0)}. \tag{6}$$

Also from Eq. (4a), the following equation is obvious:

$$\frac{1}{g(\nu_n)I(\nu_n,z)}\frac{\mathrm{d}I(\nu_n,z)}{\mathrm{d}z}=\frac{1}{g(\nu_0)I(\nu_0,z)}\frac{\mathrm{d}I(\nu_0,z)}{\mathrm{d}z},$$

$$G(\nu_n,z)=\xi(\nu_n)G(\nu_0,z), \tag{7}$$

where $\xi(\nu_n)=g(\nu_n)/g(\nu_0)=\sigma_e(\nu_n)/\sigma_e(\nu_0)$. By using Eq. (7) and letting $I_{sd}(\nu_0)$ be the seeding intensity, the following formulas are obtained:

$$I(\nu_n,z)=(1-\eta)\eta^n I_{sd}(\nu_0)\exp\left[G(\nu_0,z)\xi(\nu_n)+G(\nu_0,L)\sum_{i=0}^{n-1}\xi(\nu_i)\right], \tag{8a}$$

$$\beta(\nu_n,z)=(1-\eta)I_{sd}(\nu_0)\frac{\eta^n}{I_s(\nu_n)}\exp\left[G(\nu_0,z)\xi(\nu_n)+G(\nu_0,L)\sum_{i=0}^{n-1}\xi(\nu_i)\right], \tag{8b}$$

where η is the efficiency of the AOM.

At the same time, from Eq. (4b), the following formula can be obtained:

$$C_p=\beta_p^{+}(z)\beta_p^{-}(z)=\beta_p^{+}(L)\beta_p^{-}(L)=\beta_p^{+}(0)\beta_p^{-}(L)\exp[\Gamma_p^{+}(L)]. \tag{9}$$

Then the total pump intensity is

$$\beta_p(z)=\beta_p^{+}(z)+\frac{C_p}{\beta_p^{+}(z)}. \tag{10}$$

Inserting Eq. (2) into Eqs. (4a) and (4b) and then combining Eqs. (4a) and (4b) gives

$$\frac{(f_p-f_l)\Sigma_n\beta(\nu_n,z)+f_p\frac{\mathrm{d}\beta(\nu_n,z)}{\mathrm{d}z}}{g(\nu_n)\beta(\nu_n,z)}=\mp\frac{(f_p-f_l)\beta_p(z)-f_l\frac{\mathrm{d}\beta_p^{\pm}(z)}{\mathrm{d}z}}{\alpha_p\beta_p^{\pm}(z)}. \tag{11}$$

In the left side of Eq. (11), let $\nu_n=\nu_0$. Inserting Eq. (8b) into Eq. (11) gives

$$\frac{(f_p-f_l)(1-\eta)I_{sd}(\nu_0)}{g(\nu_0)}\sum_n\frac{\eta^n}{\xi(\nu_n)I_s(\nu_n)}\times\exp\left[G(\nu_0,L)\sum_{i=0}^{n-1}\xi(\nu_i)\right]\frac{\mathrm{d}}{\mathrm{d}z}\exp[G(\nu_0,z)\xi(\nu_n)]=\mp\frac{(f_p-f_l)\beta_p(z)-f_l\frac{\mathrm{d}\beta_p^{\pm}(z)}{\mathrm{d}z}}{\alpha_p\beta_p^{\pm}(z)}-\frac{f_p}{g(\nu_0)}\frac{\mathrm{d}\ln\beta(\nu_0,z)}{\mathrm{d}z}. \tag{12}$$

In Eq. (6), take $z=L$; then the value of $G_p^{+}(L)$ is

$$\Gamma_p^{+}(L)=\alpha_p\left[\frac{G(\nu_0,L)}{g(\nu_0)}-(f_p-f_l)L\right]. \tag{13}$$

Using different pump methods, whose schemes are shown in Fig. 3, integrating Eq. (12) from 0 to L and then inserting Eq. (13) into it results in

(1) Single-pass pump (SPP):

$$\frac{(1-\eta)I_{sd}(\nu_0)}{g(\nu_0)}\sum_n\frac{\eta^n}{\xi(\nu_n)I_s(\nu_n)}\exp\left[G(\nu_0,L)\sum_{i=0}^{n-1}\xi(\nu_i)\right]\times\{\exp[G(\nu_0,L)\xi(\nu_n)]-1\}=\frac{\beta_p^{+}(0)}{\alpha_p}\left(1-\exp\left\{\alpha_p\left[\frac{G(\nu_0,L)}{g(\nu_0)}-(f_p-f_l)L\right]\right\}\right)-\frac{G(\nu_0,L)}{g(\nu_0)}-f_lL, \tag{14a}$$

(2) Contrapropagating pump (CPP):

$$\frac{(1-\eta)I_{sd}(\nu_0)}{g(\nu_0)}\sum_n\frac{\eta^n}{\xi(\nu_n)I_s(\nu_n)}\exp\left[G(\nu_0,L)\sum_{i=0}^{n-1}\xi(\nu_i)\right]\times\{\exp[G(\nu_0,L)\xi(\nu_n)]-1\}=\frac{\beta_p^{+}(0)+\beta_p^{-}(L)}{\alpha_p}\times\left(1-\exp\left\{\alpha_p\left[\frac{G(\nu_0,L)}{g(\nu_0)}-(f_p-f_l)L\right]\right\}\right)-\frac{G(\nu_0,L)}{g(\nu_0)}-f_lL, \tag{14b}$$

(3) Backreflected pump (BRP):

$$\frac{(1-\eta)I_{sd}(\nu_0)}{g(\nu_0)}\sum_n\frac{\eta^n}{\xi(\nu_n)I_s(\nu_n)}\exp\left[G(\nu_0,L)\sum_{i=0}^{n-1}\xi(\nu_i)\right]\times\{\exp[G(\nu_0,L)\xi(\nu_n)]-1\}+\frac{G(\nu_0,L)}{g(\nu_0)}+f_lL=\frac{\beta_p^{+}(0)}{\alpha_p}\left(1-\exp\left\{\alpha_p\left[\frac{G(\nu_0,L)}{g(\nu_0)}-(f_p-f_l)L\right]\right\}\right)\times\left(1+R_m\exp\left\{\alpha_p\left[\frac{G(\nu_0,L)}{g(\nu_0)}-(f_p-f_l)L\right]\right\}\right), \tag{14c}$$

where R_m is the reflectivity of the pump beam at $z=L$.

Now, by using Eqs. (14a)–(14c), the values of $G(\nu_0,L)$ using different pump methods can be solved numerically. When the value $G(\nu_0,L)$ is known, the output intensity is [6]

$$F(t)=I_{sd}(\nu_0)\left|\sqrt{\eta}\cos(2\pi\nu_{-1}t)+(1-\eta)\times\sum_n\sqrt{\eta^n\exp\left[G(\nu_0,L)\sum_{i=0}^{n}\xi(\nu_i)\right]}\cos(2\pi\nu_nt)\right|^2. \tag{15}$$

In this paper, they were concerned with, for the same incident pump power, the performance of the pulse laser using different pump methods. Therefore, Eqs. (14a) and (14b) are the same since $\beta_p^+(0)$ in Eq. (14a) and $[\beta_p^+(0)+\beta_p^-(L)]$ in Eq. (14b) are the incident pump intensity. That means the generated pulse lasers are the same for the SPP and CPP, and so in the following, only the performance of the SPP and BRP is studied.

3. RESULTS AND ANALYSIS

The spectral parameters of the Yb^{3+}:YAG crystal and other parameters are listed in Table 1 and used in the following analysis unless otherwise stated. Here, the emission cross section is assumed to be $\sigma_e(\nu_n)=\sigma_e(\nu_c)/[1+(\nu_n-\nu_c)^2/(0.5\Delta\nu)^2]$, corresponding to the homogeneously broadened amplifier, where ν_c is the center frequency of the emission band and $\Delta\nu$ is the full width at half-maximum (FWHM) of the emission band and is calculated by the linewidth near 1030 nm in the fluorescence spectra [8].

In Fig. 4, the peak intensities for the SPP and BRP varying with the seeding intensity are plotted; at the same time, the inset represents the difference of the peak intensities of the cases. It seems that if the seeding intensity is not very high, high peak intensities do not result. For both pump methods, the optimum seeding intensities are almost the same and the peak intensity for the BRP is always higher than that for the SPP. For the high seeding intensity, the peak intensities under the two pump methods are almost the same and increase.

From Eq. (15), the peak intensity is mainly determined by the seeding intensity $[I_{sd}(\nu_0)]$, the efficiency of the AOM (η), the gain $[G(\nu_0,L)]$, and the number of the frequency participating in the interference (n). At the same time, the gain is affected by the seeding wavelength (ν_0), the amplifier length (L), and the number of the frequency. For the same seeding intensity, the gain of the BRP is always higher than that of the SPP since the BRP absorbs more pump power, and so the peak intensity is higher. When the seeding intensity increases, the gain always decreases. That is why the peak intensity increases to the maximum and then decreases. This is the same result as that of [6]. As expected in [6], since the seeding intensity is very high, the gain medium acts as a transparent medium, and that means the gain is zero, and so the peak intensity varies linearly with the seeding intensity.

Table 1. Spectral Parameters of Yb^{3+}:YAG and Other Parameters

Parameters	Values
σ_p@940 nm	0.76×10^{-20} cm^2 [8]
σ_e@1030 nm	2.3×10^{-20} cm^2 [8]
ν_c	c/1030 nm
$\Delta\nu$	3.0×10^{12} Hz ($\Delta\lambda=10$ nm) [8]
τ_f	1.0 ms[8]
$f_{li}, f_{uj}, f_{lm}, f_{un}, f_p, f_l$ (300 K)	0.875, 0.169, 0.0463, 0.702, 0.838, 0.0619
λ_0	1032 nm
$\delta\nu$	100 MHz
N_0	3 at. % (4.158×10^{20} ions/cm^3)
L	5 mm
I_{p0}	10 kW/cm^2
I_0	10 kW/cm^2
η	0.96
R_m	1

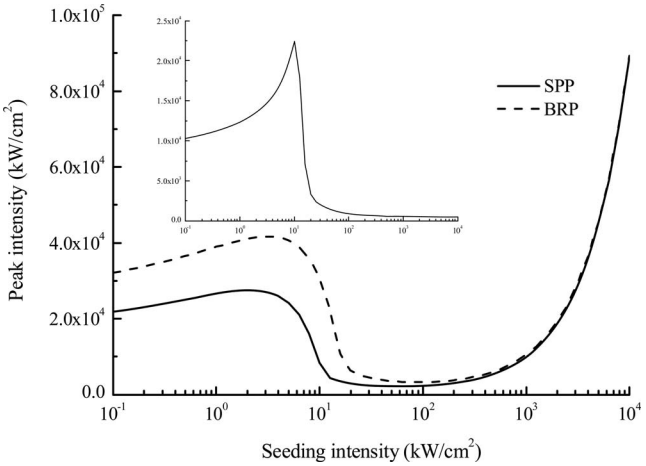

Fig. 4. Peak intensities of the SPP and the BRP vary with the seeding intensity.

Figure 5 shows the peak intensities versus the seeding frequency (also seeding wavelength $\lambda_0=c/\nu_0$) under different pump methods. The short seeding wavelength means high gain and a small number of the frequency participating in the interference; the long seeding wavelength means low gain and a large number of the frequency; therefore, there is an optimal seeding wavelength for each pump methods that is shown in Fig. 5. The figure shows that the optimal seeding wavelength is about 1032 nm and the corresponding difference between the peak intensities of the BRP and the SPP achieves maximum. If the seeding wavelength decreases from the optimal value, the peak intensity changes abruptly; moreover, the variation of the BRP is more abrupt than that of the SPP. This for the BRP, the technique stabilizing the seeding wavelength may be needed.

Figure 6 presents the effect of the amplifier length on the peak intensity. There are optimum amplifier lengths due to the reabsorption of the Yb^{3+} ion. The optimal am-

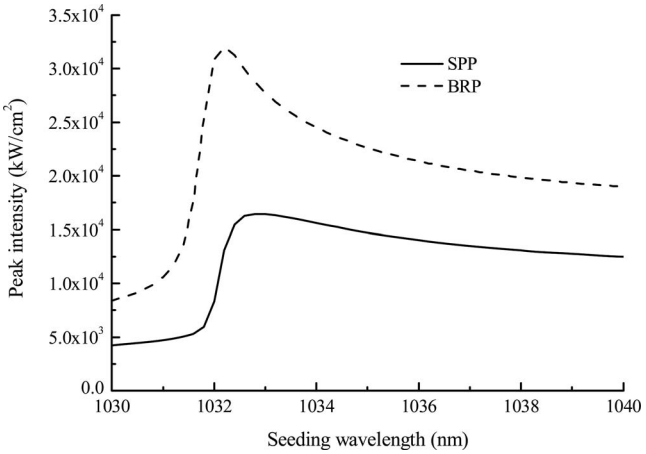

Fig. 5. Peak intensities under different pump methods vary with the seeding wavelength.

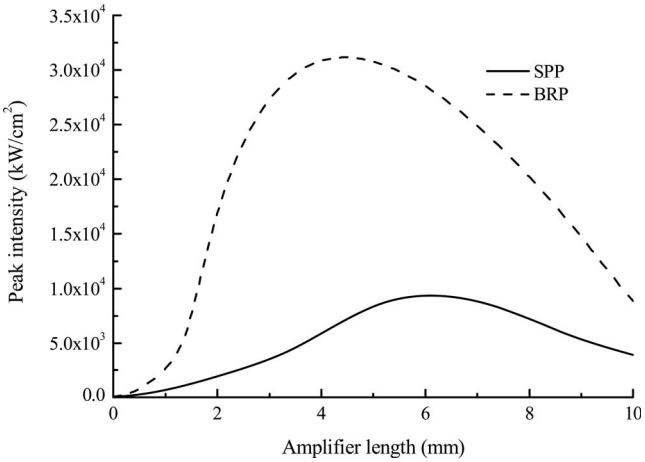

Fig. 6. Plots of the peak intensities of the SPP and the BRP vary with the amplifier length.

plifier length of the BRP is shorter than that of the SPP, and it favors the microchip material. In fact, Yb^{3+}:YAG crystal used as microchip materials has been reported [3].

Finally, the effect of the efficiency of the AOM on the peak intensity is also studied, and the results are plotted in Fig. 7. In this figure, with the efficiency increases, the number of the frequency will increase though the gain decreases. This implies that there is an optimal efficiency, as shown in the figure. It seems that the optimal efficiency is very close to 1. If the efficiency is 1, the peak intensity is the seeding intensity since no laser is amplified in the ring cavity. This figure also represents the abrupt variation of the peak intensity for both pump methods versus the optimal AOM's efficiency.

4. CONCLUSIONS AND DISCUSSIONS

In this paper, the performance of the laser pulse from an active continuous-wave-injected ring cavity with Yb^{3+}:YAG using different end-pump methods is studied, taking the saturation of the pump absorption into account. The results show that, under the same conditions, the peak intensity of the BRP is always higher than that of the SPP since the BRP absorbs more pump power. Both pump methods have optimal seeding intensity, seeding frequency, amplifier length, and efficiency of the AOM, where the optimal seeding frequency, seeding wavelength, and AOM's efficiency are almost the same. Regarding those optimal parameters' values, the peak intensity changes abruptly and that of the BRP varies more abruptly than that of the SPP. Therefore, the optimum parameters' values affect the peak intensity of the BRP more greatly than that of the SPP.

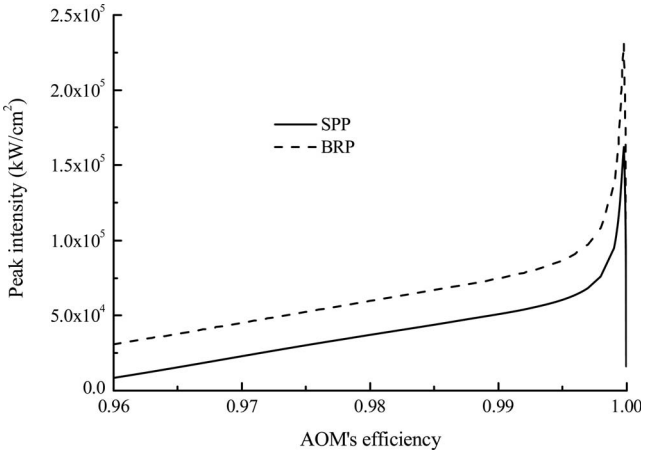

Fig. 7. Peak intensities of different pump methods vary with the efficiency of the AOM.

Recently, Yb^{3+}:LSO (Yb^{3+}:Lu_2SiO_5) crystal has received much attention since its emission band can be as broad as several dozen nanometers, and it thus is a very good amplifier for ultrashort-pulse lasers [9,10]. However, Yb^{3+}:LSO is an inhomogeneously broadened amplifier and the results of this paper do not apply to it. Therefore, further consideration should be made to deal with Yb^{3+}:LSO crystal.

ACKNOWLEDGMENTS

This work was supported by the Fujian Provincial Department of Science and Technology grant 2007F5042. Also, the author thanks Gilbert L. Bourdet of the Ecole Polytechnique, Palaisau, France for his helpful discussion.

REFERENCES

1. A. Brenier and G. Boulon, "Overview of the best Yb^{3+}-doped laser crystals," J. Alloys Compd. **323–324**, 210–213 (2001).
2. W. F. Krupke, "Ytterbium solid-state lasers—the first decade," IEEE J. Sel. Top. Quantum Electron. **6**, 1287–1296 (2000).
3. G. J. Spühler, R. Paschotta, M. P. Kullberg, M. Graf, M. Moser, E. Mix, G. Huber, C. Harder, and U. Keller, "A passive Q-switched Yb:YAG microchip laser," Appl. Phys. B **72**, 285–287 (2001).
4. G. L. Bourdet, R. A. Muller, G. M. Mullot, and J. Y. Vinet, "Short pulse generation by use of an active multipass interometer," IEEE J. Quantum Electron. **24**, 580–584 (1988).
5. G. L. Bourdet, "Short-pulse generation at 10 μm in an active cw-injected ring laser cavity," Appl. Opt. **42**, 5457–5462 (2003).
6. Z. Huang and G. L. Bourdet, "Theoretical study of cw to short pulse conversion in an active cw-injected ring cavity with a Yb^{3+}:YAG amplifier," Appl. Opt. **46**, 2703–2708 (2007).
7. G. L. Bourdet, "Theoretical investigation of quasi-three-level longitudinally pumped continuous wave lasers," Appl. Opt. **39**, 966–971 (2000).
8. J. Dong, M. Bass, Y. Mao, P. Deng, and F. Gan, "Dependence of the Yb^{3+} emission cross section and lifetime on temperature and concentration in yttrium aluminum garnet," J. Opt. Soc. Am. B **20**, 1975–1979 (2003).
9. M. Jacquemet, C. Jacquemet, N. Janel, F. Druon, F. Balembois, P. Georges, J. Petit, B. Viana, D. Vivien, and B. Ferrand, "Efficient laser action of Yb:LSO and Yb:YSO oxyorthosilicates crystals under high-power diode-pumping," Appl. Phys. B **80**, 171–176 (2005).
10. F. Thibault, D. Pelenc, F. Druon, and P. Georges, "Very efficient diode-pumped Yb^{3+}:Y_2SiO_5 and Yb^{3+}:Lu_2SiO_5 femtosecond laser," *in Conference on Lasers and Electro-Optics Europe* (CLEO) **3**, 2070–2072 (2005).